

Grain Subdivision Mechanism For Constructing Lamellar Microstructure In Cold-Rolled Ultra-Low Carbon Steel

Morikawa, Tatsuya
Department of Materials, Kyushu University

Kurosaka, Ryuta
Graduate Student, Kyushu University

Tanaka, Masaki
Department of Materials, Kyushu University

Ichie, Takeru
Nippon Steel Corporation

他

<https://hdl.handle.net/2324/7172330>

出版情報 : ISIJ International. 62 (2), pp.335-335, 2022-02-16. 日本鉄鋼協会
バージョン :
権利関係 : © 2022 The Iron and Steel Institute of Japan.



Grain Subdivision Mechanism For Constructing Lamellar Microstructure In Cold-Rolled Ultra-Low Carbon Steel

Tatsuya MORIKAWA,^{1)*} Ryuta KUROSAKA,²⁾ Masaki TANAKA,¹⁾ Takeru ICHIE³⁾ and Ken-ichi MURAKAMI⁴⁾

1) Department of Materials, Kyushu University, 744 Motooka, Fukuoka, Japan.

2) Graduate Student, Kyushu University. Now at Nippon Steel Corporation, 1-8 Fuso-cho, Amagasaki, Japan.

3) Nippon Steel Corporation, 1-1 Tobihatacho, Kitakyushu, Japan.

4) Nippon Steel Corporation, 20-1 Shintomi, Futtsu, Japan.

(Received on July 4, 2021; accepted on August 31, 2021)

To clarify the formation process of a lamellar microstructure during rolling, we employ a method for following the crystal orientation distribution in the same region before and after the rolling process, in addition, the local strain distribution owing to the formation of the rolled structure was investigated by measuring the amount of strain in the grain from cold rolling using nano-order fine markers applying a focused ion beam (FIB).

During rolling at a 50% to 70% reduction in thickness, different crystal rotations were observed in the initial grains. A trace analysis of the slip band suggested that the crystal rotation in different directions was caused by the activation of different slip systems in each region. The distribution of the equivalent plastic strain from a 60% to 70% reduction owing to a grain subdivision was examined and compared with the change in crystallographic orientation, suggesting that non-uniform slippage deviating from the Taylor model occurred in the regions where a significant orientation change occurred.

Furthermore, the strain distribution measured by the marker showed that tensile deformation caused by rolling tended to be suppressed compared to compressive deformation near the grain boundaries inclined toward the rolling direction. These results suggest that the local crystal rotation inside the grain, which leads to a grain subdivision during rolling, is caused by a deviation of the strain tensor inside the grain from the ideal rolling state.

KEY WORDS: cold rolling; strain distribution; grain boundary; slip system.

1. Introduction

The development of a preferential crystallographic orientation distribution (development of texture) in thin steel plates significantly affects the processing and electrical properties of the plates, and an elucidation of the principles for controlling that is one of the important issues in steel research. The crystallographic orientation of steel sheets can be measured using diffraction methods such as X-ray diffraction and scanning electron microscopy-electron backscatter diffraction (SEM-EBSD). Dislocation substructures are often observed in rolled plate, which develop in an inhomogeneous manner with increasing strain,¹⁻⁴⁾ and the crystal orientation changes locally with the formation of such substructures. It is known that narrow regions in these microstructures have a relatively large misorientation from the surrounding regions and become the initial region for recrystallization by heat treatment after rolling.

To understand the formation mechanism of a preferential crystallographic orientation during the early stage of recrystallization,^{5,6)} it is important to understand the features of inhomogeneous microstructures in the cold-rolled plates.

These inhomogeneous deformation structures often spread multiple grains, such as large shear bands,⁷⁻¹¹⁾ or are formed inside a single grain, such as microbands.^{1,2,12)} Such deformation structures formed inside a grain are thought to contribute to a grain refinement. For example, grain subdivision accompanied by the formation of lamellar microstructures parallel to the rolling direction is observed in a severe plastic deformation such as the accumulative roll bonding (ARB) process.¹³⁾ In the ordinary rolling process, it is known that a structure called a lamellar boundary develops with an increase in the thickness reduction with a significant development of texture,¹⁴⁾ which is thought to be accompanied by a subdivision of the initial grain. It is believed that the grain subdivision is the result of the activity of different slip systems in the grain.¹⁵⁾ Some boundary regions must then be created in the area between these regions to bear the dif-

* Corresponding author: E-mail: morikawa@zaiko.kyushu-u.ac.jp

ference in orientation. If this process is repeated, the initial grain will be divided, and the original orientation will have several new orientations. This is thought to be related to the development of a preferred orientation. In other words, with rolling, the development of an inhomogeneous deformation structure promotes the subdivision in the grains, which in turn contributes to the development of a texture. This idea is also widely accepted as the mechanism of grain refinement owing to severe plastic deformation, as described earlier. However, there is no experimental evidence that such a scenario occurs during in the rolling process.

In this study, in order to investigate the formation process of an inhomogeneous deformation microstructure from rolling, we found a method for following the crystal orientation distribution in the same region before and after the additional rolling process. We then observed how the local orientation changes at a moderate rolling rate (approximately 70%) throughout the thickness of the rolled plate. The existence of a group of grains divided into several regions, where each region changes into a different orientation, was also observed. In addition, in order to quantitatively measure the amount of strain in the grains owing to cold rolling, nano-order precise markers were regularly placed on the sides of the plate using a focused ion beam (FIB). The displacement of the markers was measured before and after the rolling process, and the local strain distribution associated with the formation of the microstructures was obtained. We focused on the grain subdivision caused by the rolling, applied markers to the grains that showed some degree of grain division, and traced the changes in their crystallographic orientation and strain distribution.

2. Experimental Procedure

Ti-added ultra-low carbon steel was employed, and had an initial grain size of approximately $50\ \mu\text{m}$ after heat treatment, the composition of which is shown in **Table 1**. The grain size was estimated using linear intercept method. The plate was cold-rolled without lubrication until its thickness was reduced by 50% and 60%, and was then cut out. The longitudinal plane was polished for observation; the deformation structure was observed using SEM, and the crystal orientation distribution was identified through SEM-EBSD. The orientation distribution was obtained over the entire thickness of the plate with a width of approximately $100\ \mu\text{m}$ in the rolling direction. For the 50% rolled material, the grains showing a tendency to divide into the areas with individual orientations were selected, and the same field of view was observed again by EBSD after additional rolling. For the 60% rolled material, a grain with the initial grain orientation split into two orientations was selected, and carbon dots with a diameter of $0.3\ \mu\text{m}$ were deposited using a focused ion beam (FIB) to be used as markers. The markers, which were arranged in a square structure, had intervals of $0.7\ \mu\text{m}$. To re-inspect the marked longitudinal plane after

additional rolling, the specimen was inserted into a mold frame before being rolled again to protect the observation surface (**Fig. 1**). Additional rolling was conducted to attain a 70% thickness reduction, and plastic strain distributions were obtained by tracing the displacement of the markers and capturing the changes in crystal orientation in the selected regions.

3. Experimental Results

Figure 2 summarizes the grain boundary spacing in the normal direction (ND) for the 75 grains whose orientation was determined using EBSD from the rolled sheet with a 50% reduction in thickness. The observed intergranular spacing was divided into $5\ \mu\text{m}$ intervals from 0 to more than $35\ \mu\text{m}$, and the distribution of the number of grains with the spacing within that range is represented. Because the initial grain size was $50\ \mu\text{m}$, the grain boundary spacing should be close to $25\ \mu\text{m}$ if the initial grains are retained at a 50% reduction in thickness. However, more than 70% of the grain boundaries had a spacing of smaller than $25\ \mu\text{m}$. This indicates that the initial grains were divided, and new grain boundaries were formed by rolling up to a 50%

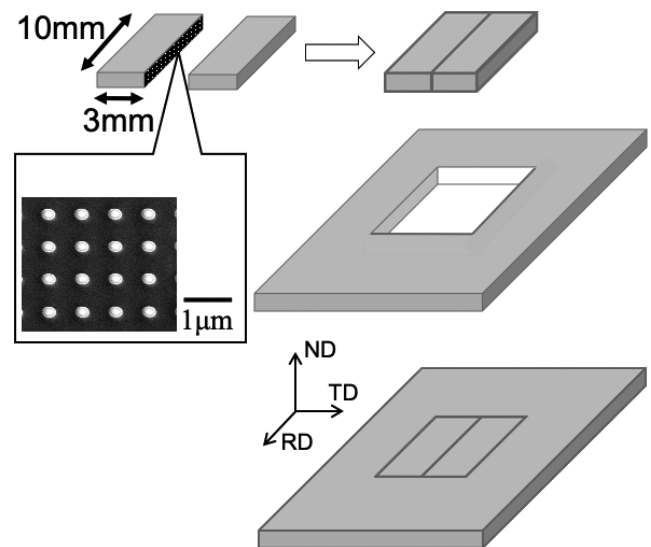


Fig. 1. Schematic diagram showing the rolling procedure.

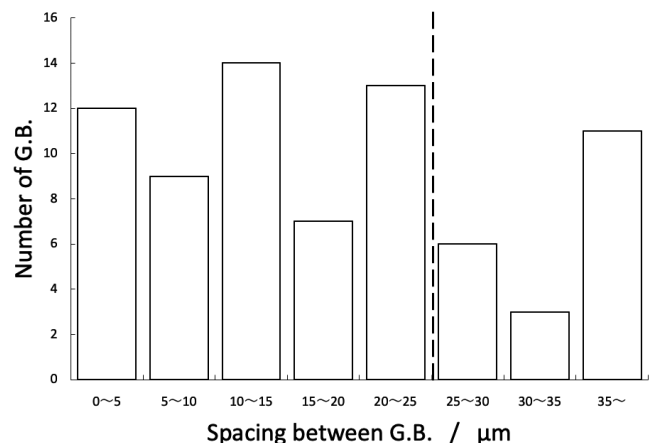


Fig. 2. Grain boundary spacing distribution in the ND direction at 50% reduction in thickness.

Table 1. Sample composition.

C	Si	Mn	P	S	Ti	Fe
0.001	<0.003	<0.003	<0.002	<0.0003	0.026	Bal.

reduction in thickness.

Figures 3(a), 3(b), and 3(c) correspond to the orientation images for the grains with different orientations inside the initial grain obtained at a 50%, 60%, and 70% reduction in thickness, respectively, and each orientation image indicates the ND. At the center of the field of view, several colored orientations appeared inside the grains at a 50% reduction. As the rolling progressed, the 100 in the red orientations and 111 in the blue orientations became dominant, and some distinct grain boundaries (with an orientation difference of more than 15°) were formed between the regions of these orientations. It can be seen that the focused grains were mostly divided into upper and lower regions, having individual orientations. Figures 3(d), 3(e), and 3(f) show the 111 pole figures of the grain at the center of the field of view obtained at a reductions of 50%, 60%, and 70%, respectively. In Fig. 3(d), each of the 111 poles is widely spread out, in Fig. 3(e), they are further dispersed, and in Fig. 3(f), they are completely separated into two poles. These orienta-

tion changes correspond well with those shown in Figs. 3(a), 3(b), and 3(c), respectively.

Figure 4(a) shows the SEM image of the TD plane at a 50% reduction in thickness, corresponding to the orientation image in Fig. 3(a). Slip bands appeared in each grain. In particular, the middle grain has slip bands in different directions in the upper and lower parts. The upper and lower regions correspond to the regions with extremely different orientations, as shown in Fig. 3(a). The initial orientation of the grain is presumed to have been split into the two new orientations shown in Fig. 3 through the activities of the different slip systems that formed these slip bands. Figures 4(b) and 4(c) show the 111 and 110 pole figures obtained from the top and bottom of the middle grain, respectively. In the figures, the center is in the transverse direction (TD), the horizontal direction corresponds to the rolling direction (RD), and the vertical direction corresponds to the ND. In the figure, the poles at reductions of 50, 60, and 70% are shown in red, yellow, and blue, respectively. There are

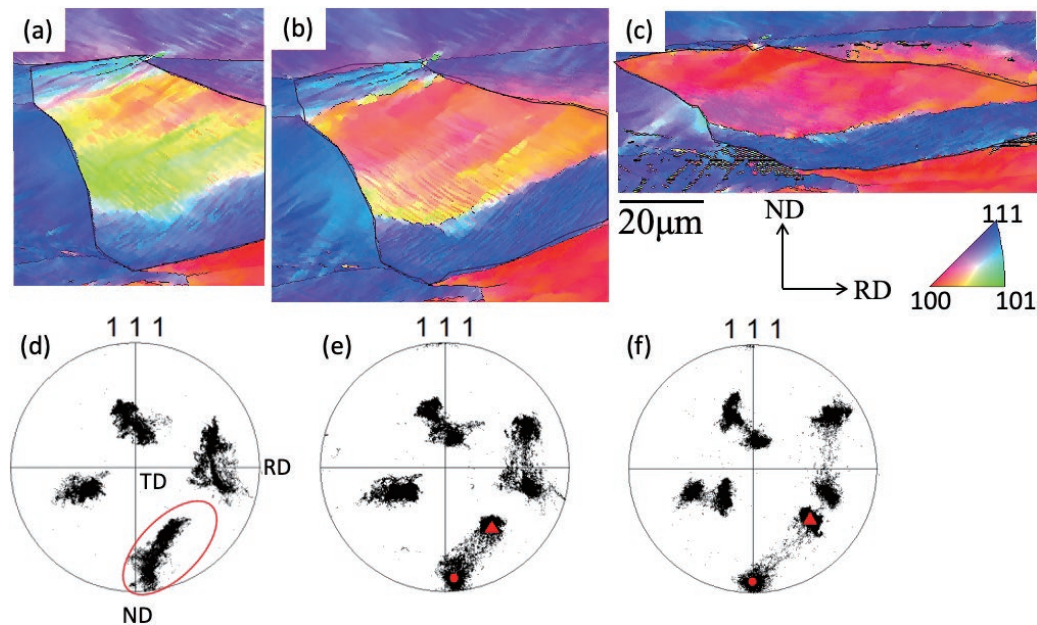


Fig. 3. Change in the orientation image in the same field of view with rolling ((a) 50% reduction, (b) 60% reduction, and (c) 70% reduction) and the 111 pole figure of the middle grain at each reduction ((d) 50%, (e) 60%, (f) 70%).

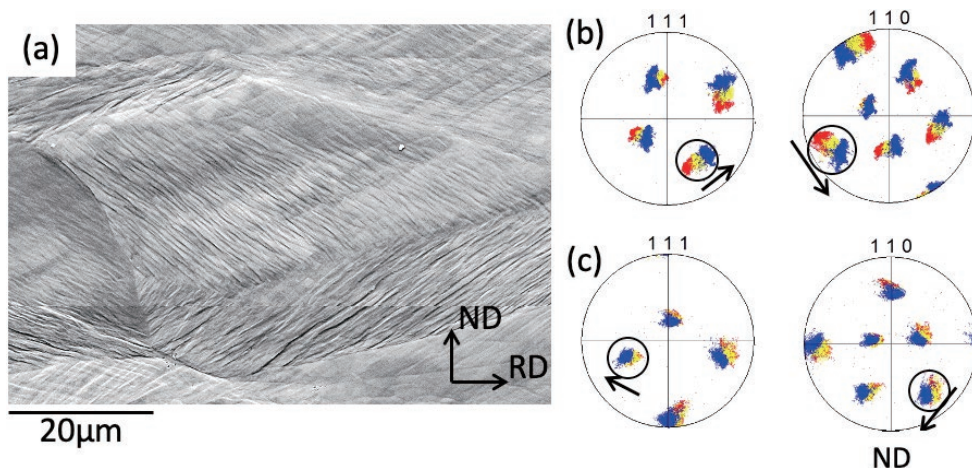


Fig. 4. (a) SEM image at 50% reduction in thickness (corresponding to Fig. 3(a)), (b) 111 and 110 pole figures of the upper region of the middle grain, and (c) 111 and 110 pole figures of the lower region of the middle grain.

four $\langle 111 \rangle$ slip directions in the bcc material. In addition, the $\langle 111 \rangle$ direction, which corresponds to the active slip system responsible for a crystal rotation, is considered to change its direction to the RD with a deformation. The circled pole in the 111 pole figure obtained from the top of the grain (Fig. 4(b)) moves toward the RD with an increasing reduction in thickness. The $\{110\}$ plane corresponding to the trace of the slip at the top of the grain shown in Fig. 4(a) is indicated by a circle in the 110 pole figure. The 110 pole moves in a direction normal to the rolling surface with rolling. Moreover, the stress factors calculated for the four possible directions of the slip system, including the circled slip plane, were 0.91, which is the largest value in the direction indicated by the circle in the 111 pole figure. These results suggest that the active slip system at the top of the grain in Fig. 4(a) was $\langle 111 \rangle \{110\}$, which is indicated by the circle in Fig. 4(b). Similarly, in the lower part of the grain in Fig. 4(a), the circled 111 and 110 poles move toward the RD and ND, respectively, with an increasing reduction in thickness, as shown in Fig. 4(c). The 110 pole is one of the slip planes corresponding to the trace of the slip bands in the SEM image. The stress factor of the slip system is 0.63, which is the largest value among the four slip systems corresponding to the four directions in the figure. The slip system at the bottom of the grain in Fig. 4(a) is considered to be the slip system indicated by the circle in Fig. 4(c). It is therefore considered that the activity of the different slip systems at the top and bottom of the grain is the main cause of the initial grain splitting.

Figures 5(a), 5(b), and 5(c), 5(d) show the orientation of the crystal parallel to the ND and RD at 60% and 70% reduction, respectively. The horizontal direction in the figure corresponds to the RD. As shown in Figs. 5(a) and 5(c), the orientations of the upper and lower regions inside the middle grain are different, and the color of the lower region of the grain changes further with an increasing reduction in thickness, indicating that the difference of orientation between the upper and lower regions increases. By contrast, in the orientation images shown in Fig. 5(b) and 5(d), the RD of the entire grain is almost $\langle 011 \rangle$. Therefore, it is clarified that the lower part of the grain of interest is rotated around the RD axis.

To clarify how the local strain changes with the change in orientation inside the grain, markers were added by FIB at a 60% reduction in thickness, and further rolled up to a 70% reduction, and the displacement of the markers was captured. Figures 6(a) and 6(b) show the orientation images of the marked area (inside the thick black line) at a 60% and 70% reduction, respectively. The grain is the same as in Fig. 5, and the shape of the region surrounded by the thick black line changes in a nonuniform manner after additional rolling. Figure 6(c) shows SEM images of dot-shaped markers applied to the surface of the specimen at a 60% reduction through an FIB carbon deposition. The spacing between the markers was set to $0.7 \mu\text{m}$. Figure 6(d) shows an SEM image of the same field of view shown in Fig. 6(c) after an additional rolling of the sample up to a 70% reduction. After the additional rolling, the markers were still attached to the longitudinal plane and their positions were non-uniformly displaced. Figure 6(e) shows the equivalent plastic strain distribution calculated from the displacement of the marker at a 70% reduction. The strain concentration region appears to be inclined toward the RD. In Fig. 6(b), the upper part of the middle grain is red, the lower part is blue, and the orientation parallel to the ND of the plate changes gently at their boundaries. Despite the change in orientation, the strain distribution shown in Fig. 6(e) was relatively uniform, and there was no significant difference between the upper and lower regions of the grains.

The relationship between the strain distribution and the change in orientation of the grains with an increasing reduction in thickness was investigated. In Figs. 6(a) and 6(b), seven locations, labeled A–G, including the region where the orientation changes significantly along the ND, are selected and surrounded by thin black lines. These regions represent the same areas before and after additional rolling. At each reduction in thickness, the average crystallographic orientation at each location was calculated from each orientation image, and the average change in orientation was calculated for each region. Table 2 shows the average orientation changes and the average strain inside each region obtained from the marker displacement. The values in the right column are described later. Except for region A, the crystallographic orientation changes in regions E–G are

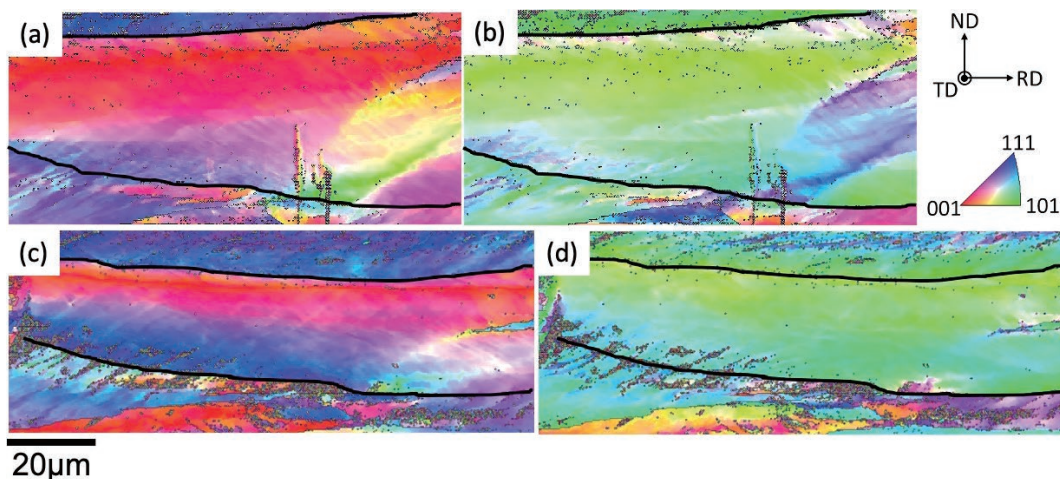


Fig. 5. (a) SEM image at 50% depressurization (corresponding to Fig. 3(a)), (b) 111 and 110 polar plots of the upper region of the middle grain, and (c) 111 and 110 polar plots of the lower region of the middle grain.

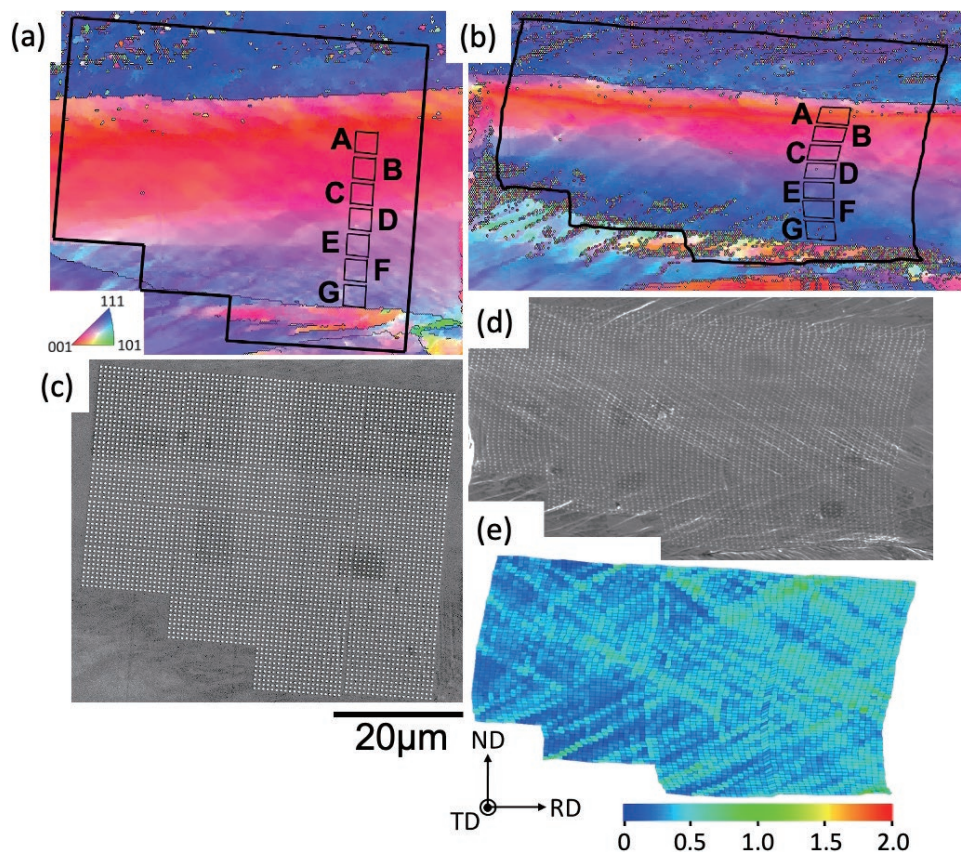


Fig. 6. Orientation image of the marked area, (a) 60% reduction and (b) 70% reduction. SEM images of the markers, (c) 60% reduction and (d) 70% reduction. (e) Distribution map showing the local strain increase between 60% and 70% reduction.

Table 2. Measured change in orientation in selected regions A–G at 60% to 70% reduction, measured mean equivalent plastic strain, and change in orientation estimated from the mean orientation at 60% reduction and mean equivalent plastic strain up to 70% reduction.

area	measured (deg.)	average strain	estimated (deg.)
A	22.7	0.44	9.3
B	5.5	0.50	6.5
C	8.3	0.41	7.3
D	10.8	0.42	7.3
E	14.9	0.39	6.0
F	16.6	0.39	6.5
G	18.5	0.36	5.6

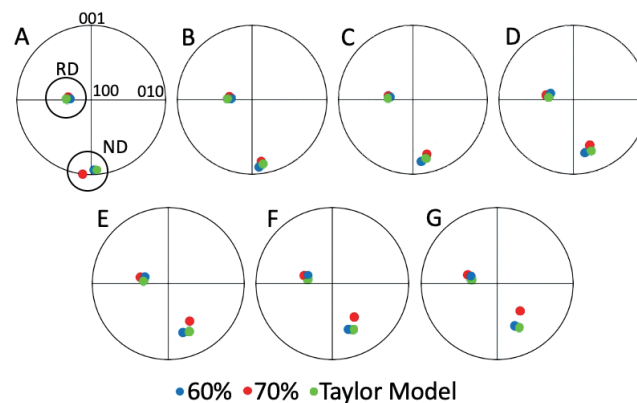


Fig. 7. 100 inverse pole diagram showing the RD and ND obtained from the experiments in regions A–G shown in Fig. 6 at a 60% and 70% reduction, and the RD and ND calculated from the Taylor model at a 70% reduction.

larger than those in the other regions. It can be inferred that the crystallographic orientation in region A changed significantly owing to the influence of the grain boundary above after additional rolling. By contrast, the average strains in regions E–G are all below 0.4, which is smaller than the average strains in regions A–D (0.4–0.5). In Fig. 6(b), the orientation of the ND in regions B–D was close to 100.

The average crystallographic orientation at a 60% reduction in thickness and the average strain induced through an additional rolling up to a 70% reduction were used to predict the crystallographic orientation at a 70% reduction, and the average crystallographic orientation was compared with the measured values. Assuming that minimizing the sum of

the shear strains owing to the four $\langle 111 \rangle$ slips based on the Taylor model, the crystal orientation can be uniquely obtained for any given normal strain.¹⁶⁾ The ND and RD of the average crystallographic orientation in the A–G region of Fig. 6 at a 60% and 70% reduction, respectively, and the ND and RD of the crystallographic orientation at 70% reduction as predicted by the Taylor model are shown in the inverse polarity diagram (A–G) in Fig. 7. It can be seen that the RD in each region has almost the same orientation. By contrast, the ND was almost the same in the areas A–D. However, in regions E–G, the measured ND at a 70% reduction is rotated by approximately 15° compared to that at a

60% reduction, despite the predicted change in orientation by the Taylor model being only a few degrees. As shown in Table 2, the values of the equivalent plastic strain in regions E–G are smaller than those in A–D. This suggests that the crystal rotation in these regions was caused by deformation deviating significantly from the Taylor model.

4. Discussion

4.1. Effect of Grain Shape on Rolling Strain Tensor

Plastic deformation inside the grains in polycrystalline materials requires the activity of at least five slip systems according to the von Mises criterion. In addition to the stress factor, which relates the external force to the shear stress on the slip plane, it is expected that material factors such as the nature of the grain boundary and the difference in orientation from the surrounding grains affect the actual activity of each slip system in the grain. This is because these factors will affect the magnitude of the resolved shear stress during the activity of each slip system. In other words, in a given region of the grain, the slip system that can act most easily will be active in that region. In this section, we focus on the grain shape as a factor affecting the activity of the slip system. As shown in Fig. 6, the upper grain boundaries of the grain are relatively parallel to the RD, whereas the lower grain boundaries, which are in contact with the region where the crystal rotation is accelerated with rolling, are inclined toward the RD. If we take an extremely simple view of the rolling deformation, it can be regarded as a plane strain condition, and can be considered as a two-dimensional problem in the longitudinal plane. Then, in the x-y plane, assuming that the x-direction is parallel to the rolling direction and that the shear strain is zero for simplicity, the strain tensor is given by

$$\begin{pmatrix} \varepsilon_{xx} & 0 \\ 0 & \varepsilon_{yy} \end{pmatrix}, (\varepsilon_{yy} = -\varepsilon_{xx})$$

After a certain amount of rolling, the many grains elongate in the rolling direction and most of the grain boundaries become parallel to the rolling plane. The finite element method was used to predict the change in the strain tensor

for grains with some of the grain boundaries inclined in the rolling direction.

Figures 8(a) and 8(b) show the distribution of ε_{xx} and ε_{yy} for the two-layered model, in which the material with a 5% higher yield strength and 5% lower work hardening rate was placed on top, and the original material was placed on the bottom. FEM software ANSYS R19.2 was used for the analysis, and the number of nodes was set to 8 000. The boundary conditions were as follows: The lower left vertex was fixed, the left side was fixed in the x direction, the lower side was fixed in the y-direction, and the upper side was subjected to a forced displacement with a strain of 0.25 downward. The higher yield strength of the upper layer corresponds to the fact that the lower part of the grain in Fig. 6 was rotated to $\{111\} \langle 011 \rangle$. Grain with a γ -fiber orientation, where the ND is parallel to $\langle 111 \rangle$, is generally considered to be relatively hardened owing to large work hardening. In fact, as shown in Table 2, the amount of plastic strain estimated for the lower region of the grain in Fig. 6 after rotation toward the γ -fiber orientation is relatively small. In Fig. 8(a), both the upper and lower layers show similar ε_{xx} values. In Fig. 8(b), the ε_{yy} of the lower layer with a lower yield strength appears to be larger than that of the upper layer, reflecting the constraints of the cal-

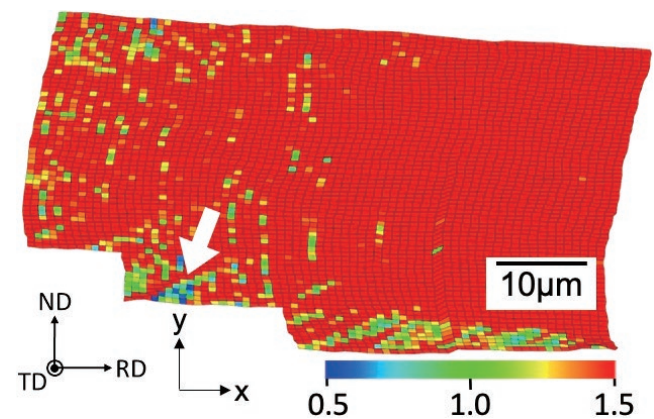


Fig. 9. Distribution of $\varepsilon_{xx}/-\varepsilon_{yy}$ values obtained from the strain as measured by the marker.

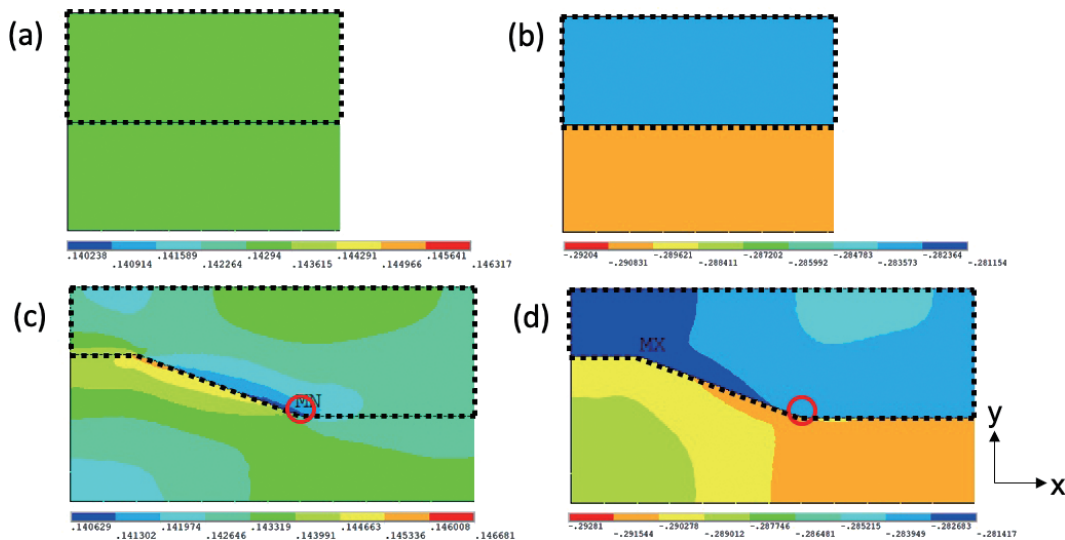


Fig. 8. Strain distribution calculated by finite element method, (a)(c) ε_{xx} and (b)(d) ε_{yy} .

ulation model.

However, Figs. 8(c) and 8(d) show a model in which the boundary conditions and displacement conditions are the same as above, whereas the shape of the grain boundary between the two layers is changed. In this model, a part of the grain boundary contains an inclined part. The analysis results show that the distributions of both ε_{xx} and ε_{yy} are non-uniform. In Fig. 8(c), a relatively small region of ε_{xx} appears in the upper layer and a large region of ε_{xx} is observed in the lower layer along the inclined grain boundary. By contrast, the opposite tendency was observed in the ε_{yy} distribution shown in Fig. 8(d). At the foot of the inclined grain boundary circled in the figure, we obtained the ratio $\varepsilon_{xx}/-\varepsilon_{yy} = 0.495$, indicating that the strain in the x-direction may be smaller than that in the y-direction.

Figure 9 shows the distribution of $\varepsilon_{xx}/-\varepsilon_{yy}$, where ε_{xx} and ε_{yy} are measured from the displacement of the marker. The shape of this figure corresponds to the area marked with a black frame in Fig. 6(b) at a 70% reduction. The value of $\varepsilon_{xx}/-\varepsilon_{yy}$ is greater than 1 in many areas in the figure, including the area near the upper grain boundary. This suggests that the deformation mode deviates from the plane strain in most of the grains, and is under a deformation mode that is tensile or compressed parallel to the TD axis. By contrast, in the region near the grain boundary, which is inclined toward the RD, as indicated by the white arrow in the figure (see Fig. 6(b)), the value of $\varepsilon_{xx}/-\varepsilon_{yy}$ is below 1. This is consistent with the calculation results shown in Fig. 8.

4.2. Crystal Rotation Contributing to Grain Subdivision

In the previous section, we suggested that the inclination of the grain boundary to the RD may affect the strain tensor inside the grain. When the normal strain in the rolling direction becomes smaller than that in the direction normal to the plate surface, the active slip system changes. In this section, we investigate how the crystal rotation changes under that situation. A rolling deformation can be considered as a combination of tensile deformation in the rolling direction and compressive deformation in the thickness direction. Then, the magnitude of the Schmid factor of the

typical slip system was calculated as the angle of deviation from the initial orientation when tension and compression were applied independently. **Figure 10(a)** shows the variation in the Schmid factor with the amount of crystal rotation about the RD axis from the initial orientation (112)[1 $\bar{1}$ 0] (ND/RD) for the major slip systems (slip systems with high Schmid factor values). The relationship between the initial orientation of the crystals of interest and the coordinate system of the rolled plate is RD//[1 $\bar{1}$ 0], ND//[112], and TD//[11 $\bar{1}$]. The Schmid factor for each slip system in a tensile deformation parallel to RD does not change with crystal rotation about the RD axis, with a maximum of 0.47 (the slip system is [111](1 $\bar{1}$ 2) and [1 $\bar{1}$ 1]($\bar{1}$ 12)), and the next largest value of 0.41 (for the slip systems [111](101) or (0 $\bar{1}$ 1) and [1 $\bar{1}$ 1]($\bar{1}$ 01) or (011)).

From Fig. 10(a), it can be seen that the values of the Schmid factor in terms of the tensile deformation are larger than those of the main slip system in a compressive deformation parallel to the ND for the initial orientation (abscissa = zero). Therefore, it is assumed that no crystal rotation from the initial orientation occurs during the ideal rolling deformation. However, when the tensile deformation is suppressed against compressive deformation near the grain boundary, as discussed in the previous section, the apparent Schmid factor for the tensile deformation of each slip system can be considered to be smaller. Alternatively, this can be thought of as a decrease in the apparent resolved shear stress of each slip system during a tensile deformation. **Figure 10(b)** shows a situation in which the Schmid factor of each slip system in a tension deformation is reduced compared to that in a compression deformation (indicated by the white arrows). In this case, [1 $\bar{1}$ 1](011), which has the largest Schmid factor in a compressive deformation, is first activated, and the crystal orientation rotates in the direction of the black arrow. Then, the additional [1 $\bar{1}$ 1](121) becomes active, and the crystal orientation may be rotated by approximately 20°. If the initial orientation (112)[1 $\bar{1}$ 0] rotates 20° around the RD, the crystal orientation becomes (111)[1 $\bar{1}$ 0], which corresponds to the observed orientation. These results suggest that the local rotation within the grain, which leads to grain subdivision during rolling, is caused

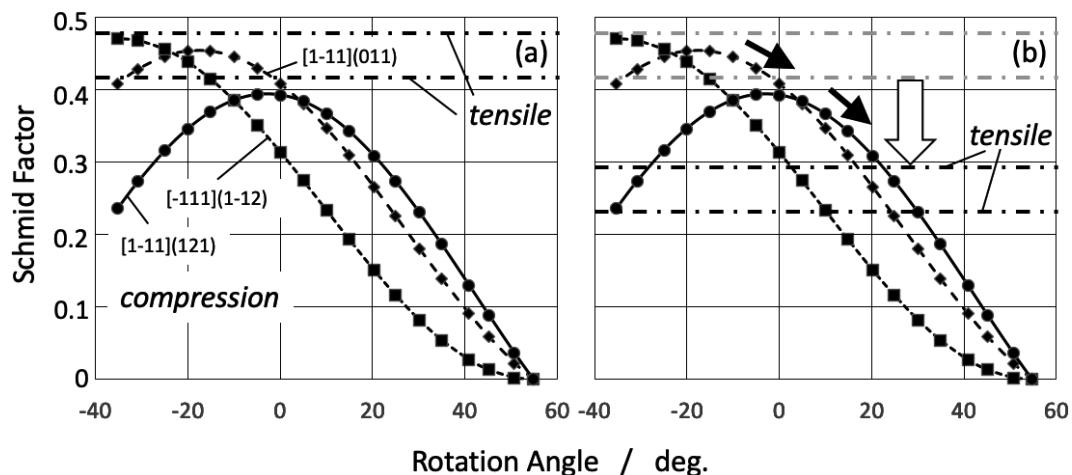


Fig. 10. (a) Change in Schmid factor of each slip system with crystal rotation about the RD axis when the initial orientation is [1-10](112) in each deformation mode of tensile and compressive rolling. (b) The apparent change in Schmid factor when the tensile deformation is inhibited.

by a deviation from the ideal rolling state. The results also indicate that this deviation may depend on the grain shape.

5. Conclusions

(1) During cold rolling at a 50% to 70% reduction in thickness, a grain subdivision was observed ex-situ owing to different crystal rotations in the initial grains at different locations. A trace analysis of the slip band suggested that the crystal rotation in different directions was caused by the activation of different slip systems in each region.

(2) Marking through carbon deposition using a focused ion beam (FIB) was applied to the longitudinal plate, and the equivalent plastic strain distribution from a 60% to 70% reduction in thickness was investigated, as associated with the grain subdivision, and compared with the change in crystal orientation.

(3) Based on the strain generated and the orientation prior to the rolling, the crystal orientation after additional rolling was predicted using a pencil glide and the full constraint Taylor model. A comparison of the estimated orientation against the measured orientation suggests that non-uniform slip deviating from the Taylor model is activated within the region where significant orientation changes occur.

(4) The strain distribution measured by the marker showed that the tensile deformation caused by rolling tended to be suppressed compared to the compressive deformation near the grain boundaries inclined toward the RD, as also

suggested through an FEM analysis.

(5) The activation of the slip system when the tensile deformation was suppressed as compared to a compressive deformation was estimated from the orientation factors, and it was shown that a crystal rotation corresponding to the observed change in orientation could occur when the compressive deformation was dominant in comparison to the tensile deformation.

REFERENCES

- 1) B. Bay, N. Hansen, D. A. Hughes and D. Kuhlmann-Wilsdorf: *Acta Metall. Mater.*, **40** (1992), 205.
- 2) N. Hansen: *Mater. Sci. Technol.*, **6** (1990), 1039.
- 3) B. L. Li, A. Godfrey, Q. C. Meng, Q. Liu and N. Hansen: *Acta Mater.*, **52** (2004), 1069.
- 4) Q. Liu, X. Huang, D. J. Lloyd and N. Hansen: *Acta Mater.*, **50** (2002), 3789.
- 5) N. Hashimoto, N. Yoshinaga and T. Senuma: *ISIJ Int.*, **38** (1998), 617.
- 6) F. J. Humphreys and M. Hatherly: *Recrystallization and Related Annealing Phenomena*, Elsevier, Oxford, UK, (2004), 169.
- 7) Q. Z. Chen and J. Duggan: *Phys. Met. Metall.*, **96** (2003), 16.
- 8) T. Morikawa, D. Senba, K. Higashida and R. Onodera: *Mater. Trans., JIM*, **40** (1999), 891.
- 9) T. Morikawa, K. Higashida and T. Sato: *ISIJ Int.*, **42** (2002), 1527.
- 10) M. Z. Qadir and B. J. Duggan: *ISIJ Int.*, **46** (2006), 1495.
- 11) S. Nakanishi, T. Morikawa, K. Higashida, H. Murakami, K. Kimura and K. Ushioda: *Tetsu-to-Hagane*, **98** (2012), 253 (in Japanese).
- 12) M. Hatherly and A. S. Malin: *Met. Technol.*, **6** (1979), 308.
- 13) Y. Saito, N. Tsuji, H. Utsunomiya, T. Sakai and R. G. Hong: *Scr. Mater.*, **39** (1998), 1221.
- 14) D. A. Hughes and N. Hansen: *Metall. Trans. A*, **24** (1993), 2022.
- 15) A. Zisman: *Int. J. Eng. Sci.*, **116** (2017), 155.
- 16) H. Kato: Ph.D. thesis, Kyoto University, (1981), (accessed 2011-04-01).